Analysis of GPS/IMU Sensor Fusion to Improve Mapping Accuracy on UAV Quadrotor Using LiDAR Technology

Cahyadi, M. N.,[1*] Navisa, S. C.,[1] Asfihani, T.,[2] Suhandri, F. H.[3] and Ramadhania, N.[4]
[1]Department of Geomatics Engineering, Institut Teknologi Sepuluh Nopember, Surabaya, Indonesia
[2]Department of Mathematics, Institut Teknologi Sepuluh Nopember, Surabaya, Indonesia
[3]Centre of Studies for Surveying Science & Geomatics, Universiti Teknologi Mara (UiTM), Shah Alam, Malaysia
[4]Department of Survey and Mapping, Politeknik Sinar Mas Berau Coal, Kalimantan Timur
**Corresponding Author*

DOI: https://doi.org/10.52939/ijg.v22i2.4785

Abstract
Unmanned Aerial Vehicles (UAVs) play a crucial role in navigation, requiring accurate sensors to determine position, speed, and orientation, especially in unknown environments. Direct navigation systems like the Global Positioning System (GPS) provide positional data, while indirect systems, such as the Inertial Measurement Unit (IMU), integrate accelerometer and gyroscope data to supply speed and orientation information. This study investigates the integration of GPS and IMU sensors using the Unscented Kalman Filter (UKF) to improve localization accuracy on a cost-effective UAV Quadrotor equipped with LiDAR Livox. The research methodology involved collecting raw data from GPS, IMU, and LiDAR sensors during UAV flights. These data were processed using a UKF-based mathematical model to fuse sensor inputs and generate accurate point cloud models. Results show that the UKF fusion method achieved a localization accuracy of 0.403 m, with maximum residuals recorded as 1.332 m for the X axis, 20.421 m for the Y axis, and 4.385 m for the Z axis, significantly outperforming standalone GPS systems. Additionally, the UKF improved the precision of 3D LiDAR point clouds, achieving an overall accuracy of 0.034 m, with specific axis accuracies of 0.007 m (X axis), 0.005 m (Y axis), and 0.032 m (Z axis). These advancements resulted in a denser point cloud, enhancing volumetric calculations by 28.92% compared to the Extended Kalman Filter (EKF). The study highlights the robustness of UKF in handling sensor noise and nonlinearities, making it a suitable approach for UAV navigation and mapping tasks. These findings support the broader application of GPS/IMU sensor fusion in cost-sensitive UAV systems, emphasizing its potential for environmental mapping, precision agriculture, and urban planning.

Keywords: 2D LiDAR, GPS/IMU, Low-cost GPS, Nonlinear System Model, Unscented Kalman Filter (UKF)

1. Introduction

Uncrewed flying vehicles, commonly called Unmanned Aerial Vehicles (UAVs), are spreading widely in the civilian market mainly due to advances in the field of microelectronics. This is evident in the recent rapid application of the devices by different civil societies such as the usage in remote sensing, traffic monitoring, agriculture, navigation, health, and logistics. UAV plays an important role in the medical field, specifically in the rapid delivery of first aid and efficient medical supplies [1]. This is due to the ability to avoid traffic congestion and provide medical treatment at minimum transportation costs and computing time. UAV is also capable of determining position with a high level of precision and this is crucial in several applications such as collecting navigation coordinates and remote sensing. The attribute allows the devices to perform georeferencing directly from aerial imagery and create orthophotos on the spot [2].

Accurate and efficient estimation of positions is an important element in autonomous or UAV flight missions [3]. UAV usually relies on the sensors that provide information on position, speed, and orientation to determine the location as well as to navigate an unknown environment. Some of these sensors such as Global Positioning System (GPS) provide direct navigation information while others including inertial sensors are indirect due to the

provision of speed and orientation data. The inertial sensors, commonly called Inertial Measurement Units (IMU), are normally produced through a combination of acceleration data (accelerometer) and angular velocity (gyroscope). It is important to state each sensor has characteristics that complement the respective shortcomings. GPS had high accuracy in determining position over a long period but the signals could not work optimally in locations where the receiver was unable to receive satellite signals such as in tunnels, buildings, or very dense forests [4]. GPS accuracy can decrease due to the number of satellites that can be accessed less than four, multipath effects, and obstruction from the external environment [5]. In addition to local environmental limitations such as multipath or signal obstruction, atmospheric phenomena can also affect GNSS data quality [6]. This confirms that extreme atmospheric conditions can be an additional source of GPS accuracy degradation in navigation and UAV mapping applications.

IMU, as a complement to GPS, does not depend on external signal interference which has the ability to block or interfere with the signal because the measurements are based on signal acceleration. The data frequency of this device also reaches a high level and can interpolate GPS positions with a short acquisition time [7]. However, IMU is prone to noise due to vibrations in the vehicle body, the effects of gravity, and offsets in the sensors which often leads to in position accuracy as the time increases [8]. This means GPS and IMU sensors can be combined to achieve increasingly higher accuracy and complete positioning due to the possibility of the characteristics complementing each other.

The method most often used recently to perform navigation data fusion is Kalman Filter which is a set of mathematical equations using an optimal prediction-correction estimator to minimize the error covariance of the estimation results [9]. It is also defined as an algorithm that uses a set of observational data to estimate unknown variables more accurately. Kalman Filter has been widely applied for position tracking, navigation integration, and sensor data fusion. The method had been applied to fuse GPS and IMU sensor data into UAV [10] and was reported to have a good horizontal position estimation accuracy with Root Mean Square Error (RMSE) of 0.6 m. The standard Kalman Filter method can only be applied to linear systems but nearly all systems are nonlinear in practice [11]. This led to the focus of a previous study on GPS and IMU sensor fusion on UAV using a State-Dependent Riccati Equation (SDRE) nonlinear filter which was further implemented to form Extended Kalman Filter (EKF) [12]. The method is applicable to nonlinear systems and has been widely adopted due to the simple calculations but the performance is also influenced by measurement noise. Errors often accumulate when the estimated covariance matrix is not sufficiently accurate and this can cause the estimation results to diverge [11]. Further modification of Kalman Filter method has led to the determination of Unscented Kalman Filter (UKF) as the solution to overcome nonlinear systems by producing estimation results considered close to the actual value, leading to a higher and convergent position accuracy. The fusion of GPS and IMU sensor data using UKF method increased position accuracy on autonomous vehicles [8]. But, The UKF shows a rougher trajectory than the EKF. This is due to the combing process in the EKF [13].

The application of LiDAR technology through UAV outperforms the usage in aircraft based on cost and time required. This is because flying UAV does not require a difficult licensing process, runway facilities, and particular types of aircraft fuel. It also ensures safety of the surveyors due to the minimal interaction with the objects being measured and absence of accident risks. LiDAR with UAV is becoming more popular with the public because of the ability to overcome the obstacles associated with airplanes. However, the use and accuracy of this new technology is not yet widely known.

GPS is normally used in LiDAR system to determine the position of flying vehicle in 3D (X, Y, Z or L, B, h) against a particular reference system [14]. The position is usually determined differentially in order to observe the position of the stationary or moving objects in real-time. This has led to the designation of GPS determination method as Real Time Kinematic Differential GPS (RTK-D GPS) [15]. Based on the results of research determining ZTD values using GNSS, ZTD values vary depending on the height of each station. The higher the location above ground level, the lower the pressure, which causes ZHD values to also be low [6]. Thus, when using GPS to determine a position, the topographical aspect of the location's height must be taken into consideration. Meanwhile, IMU is a navigation system that is capable of detecting the changes in geography, speed, and orientation of an object. This system has the ability to measure the magnitude of the change in the orientation angle of flying vehicle towards the north, the movement magnitude of the rotation angle about the horizontal axes, the acceleration, and the temperature and pressure of the surrounding air. It also produces information in the form of three-dimensional orientation and the position of flying vehicle. The application of both sensors in LiDAR mapping without filtering is expected to cause noise which has

the ability to influence the precision and accuracy. Therefore, this study aimed to conduct a visual analysis on LiDAR results using GPS/IMU fused through UKF method to produce more accurate mapping. The results are expected to provide an overview of the use and accuracy of UAV using coordinates produced through GPS/IMU fusion.

2. GPS/IMU Sensor Integration Algorithm

2.1 UAV Quadrotor Model

Kinematic equation was used to define the relationship between an angular velocity and changes in Euler velocity of an object. It was applied because the rotational motion required Euler angle but not needed in the Newton-Euler equation model. Therefore, kinematic equations were applied to convert Euler speed into the object angular speed as expressed in Equations 1 to 6 [16]:

$$\dot{\varphi} = p + q\sin\varphi\tan\theta + r\cos\varphi\tan\theta \quad \text{Equation 1}$$

$$\dot{\theta} = q\cos\varphi - r\sin\varphi \quad \text{Equation 2}$$

$$\dot{\psi} = -q\frac{\sin\varphi}{\cos\theta} \pm r\frac{\cos\varphi}{\cos\theta} \quad \text{Equation 3}$$

$$\dot{x} = U\cos\theta\cos\psi - V\left(\cos\varphi\sin\psi - \cos\psi\sin\varphi\sin\theta\right) + W\left(\sin\varphi\sin\psi + \cos\varphi\cos\psi\sin\theta\right) \quad \text{Equation 4}$$

$$\dot{y} = U\cos\theta\sin\psi + V\left(\cos\varphi\cos\psi + \sin\psi\sin\varphi\sin\theta\right) - W\left(\sin\varphi\cos\psi - \cos\varphi\sin\psi\sin\theta\right) \quad \text{Equation 5}$$

$$\dot{z} = -U\sin\theta + V\cos\theta\sin\varphi + W\cos\varphi\cos\theta \quad \text{Equation 6}$$

The parameters φ, θ, *and* ψ in equations 1-3 represent the Euler angles for roll, pitch, and yaw, respectively. The variables *p, q and r* are the angular velocities along the x, y, and z axes in the body frame. Meanwhile, $\dot{\varphi}$, $\dot{\theta}$, and $\dot{\psi}$ represent the time derivatives of the Euler angles.

The parameters *U, V*, and *W* in equations 4-6 represent the linear velocities along the x, y, and z axes in the body frame. The variables x, y, and z are the positions in the global coordinate system, while $\dot{x}$, $\dot{y}$ and $\dot{z}$ are the time derivatives of these positions. Trigonometric functions cos and sin are used to calculate the velocity components.

Quadrotor dynamics were derived from rotational and translational kinematic based on the assumption that quadrotor was a rigid body in three dimensions with 6 degrees of freedom. Moreover, the translational motion in the equation was obtained through Newton second law. The dynamics of quadrotor translation on TAK object based on the forces acting in the local horizon. TAK object is mentioned in the context of the translational dynamics equations of a quadrotor. The term describes the "drag vector," which represents aerodynamic drag forces acting on the quadrotor. These forces are part of the calculations influencing translational motion in the local horizon coordinate system. In the equations presented (Equations 7-9), the drag vector, associated with D_x, D_y and D_z, contributes to determining translational accelerations along the x, y, z and z axes. his is alongside gravitational forces and thrust (T). Scientifically, the TAK object is a functional representation used to model the aerodynamic drag forces acting on the quadrotor during flight. These forces are incorporated into the total force calculations within the translational dynamics system to accurately simulate the quadrotor's motion. The TAK object is a representation of the aerodynamic drag force vector acting on a quadrotor in its translational dynamics, computed based on the magnitude and direction of forces affecting acceleration along the local x, y, and z axes. Equations 7 to 9 express the time derivatives of the linear velocities in x, y, and z directions:

$$\dot{u} = rv - qw - g\sin\theta - \frac{D_x}{m} \quad \text{Equation 7}$$

$$\dot{v} = pw - ru + g\sin\varphi\cos\theta - \frac{D_y}{m} \quad \text{Equation 8}$$

$$\dot{w} = qu - pv + g\cos\varphi\cos\theta - \frac{D_z + T}{m} \quad \text{Equation 9}$$

The parameters D_x, D_y, and D_z in Equations 7 to 9 represent the drag forces along the x, y, and z axes. The variables m is the mass of the quadrotor, T is the thrust generated by the propeller, and g is the acceleration due to gravity. The variables $\dot{u}$, $\dot{v}$, and $\dot{w}$ are the time derivatives of the linear velocities.

The drag vector on TAK object and T is the force based on the D_x, D_y, and D_z. Meanwhile, Euler equations were used as a reference for rotational movements. The external moment used was the moment produced from the difference in force from the rotor. Quadrotor also generally produced gyroscopic torque but was ignored due to its smaller value compared to others [17]. Therefore, the equation of rotational motion was derived from Euler Law as expressed in Equations 10 to 12:

$$\dot{p} = \frac{I_{yy} - I_{zz}}{I_{xx}} qr + \frac{L}{I_{xx}}$$

Equation 10

$$\dot{q} = \frac{I_{zz} - I_{xx}}{I_{yy}} pr + \frac{M}{I_{yy}}$$

Equation 11

$$\dot{r} = \frac{I_{xx} - I_{yy}}{I_{zz}} pq + \frac{N}{I_{zz}}$$

Equation 12

The parameters I_{xx}, I_{yy}, and I_{zz}, in Equations 10 to 12 are the moments of inertia along the x, y, and z axes. The variables L, M and N represent the moment forces (torques) acting along the x, y and z axes. Meanwhile, $\dot{p}$, $\dot{q}$, and $\dot{r}$ are the time derivatives of the angular velocities.

The application of Euler angle in the equation caused a limitation when the angle $\theta = \pm\pi/2$, thereby leading to the introduction of quaternions as the solution. However, quadrotor does not generally reach the angle and this means the usage of Euler angle is not expected to produce problems during the simulation.

Kinematic equation 1- equation 6 and Quadrotor dynamics in Equations 7 to 9 are continuous time dynamic system models and required to be changed to a discrete-time dynamic system model to achieve the fusion of GPS and IMU sensor data using UKF algorithm. This discretization was applied to all the 12 state variables to be estimated, including *x0307, ẏ, ż,* $\dot{\varphi}$, $\dot{\theta}$, $\dot{\psi}$ from the kinematic model in equation 1- equation 6 and *u̇, v̇, ẇ, ṗ, q̇,* and $\dot{r}$ from the dynamic model in Equations 7 to 9. The results obtained from the process is presented in Equation 13.

The discrete-time dynamic system model formed was observed not to have any noise, found to be nonlinear because each variable depended on the others, and discovered to be in a large state space. This simply showed that there was the need for UKF method in the estimation process.

$$\begin{bmatrix} x_{k+1} \\ y_{k+1} \\ z_{k+1} \\ \varphi_{k+1} \\ \theta_{k+1} \\ \psi_{k+1} \\ u_{k+1} \\ v_{k+1} \\ w_{k+1} \\ p_{k+1} \\ q_{k+1} \\ r_{k+1} \end{bmatrix} = \begin{bmatrix} \Delta t \cdot \dot{x}_k + x_k \\ \Delta t \cdot \dot{y}_k + y_k \\ \Delta t \cdot \dot{z}_k + z_k \\ \Delta t \cdot \dot{\varphi}_k + \varphi_k \\ \Delta t \cdot \dot{\theta}_k + \theta_k \\ \Delta t \cdot \dot{\psi}_k + \psi_k \\ \Delta t \cdot \dot{u}_k + u_k \\ \Delta t \cdot \dot{v}_k + v_k \\ \Delta t \cdot \dot{w}_k + w_k \\ \Delta t \cdot \dot{p}_k + p_k \\ \Delta t \cdot \dot{q}_k + q_k \\ \Delta t \cdot \dot{r}_k + r_k \end{bmatrix}$$

Equation 13

2.2 Unscented Kalman Filter (UKF)

UKF was produced by modifying Kalman Filter in order to calculate nonlinear systems in 1997. It was also explained as an alternative estimation method to overcome complex nonlinear systems [18]. UKF is different from EKF developed to estimate nonlinear systems using an analytical linearization approach. This is mainly because the method uses the Unscented Transform (UT) to determine the mean and covariance values, thereby enabling estimates to be made without linearizing the measurement model [19]. Similarly to the vehicle and tyre parameters, the EKF/UKF covariance matrices usually remain constant over time, and can be tuned through Bayesian optimisations to find desirable trade-offs for a catalog of maneuvers [20]. The EKF effectively handles measurement noise but heavily relies on initial conditions for addressing highly nonlinear problems [21]. The method usually calculates the statistics of random variables experiencing nonlinear transformation [18]. The interpretation of the logic associated with UKF algorithm processing is presented in the following Figure 1.

In Figure 1, x is the state vector estimated using the Equation 14 [22]:

$$f(x_k) + w_k$$

Equation 14

Where: x is a sigma point with dimension $2L+1$, L is the dimension of the state vector, λ is a scaling parameter, and α is a constant that determines the distribution of sigma points around $x\alpha$ is generally defined as a positive number with a small value (example $1 \leq \alpha \leq 10^{-4}$), κ is a secondary scaling parameter usually denoted as $3 - L$, and W^c is the weight of the covariance.

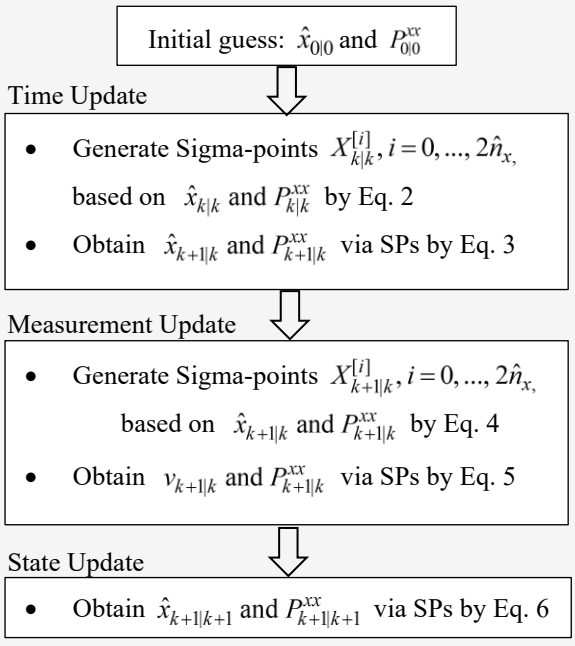

Figure 1: UKF algorithm

The EKF is an extension of the standard Kalman Filter designed to handle nonlinear systems. While the traditional Kalman Filter assumes that both the system model and the measurement model are linear, the EKF extends this applicability by linearizing these models around the current estimate using first-order Taylor expansion. In the EKF, the system dynamics are represented by a nonlinear state-space model:

$$x_{k+1} = f(x_k, u_k) + w_k, z_k = h_{(xk)} + v_k$$

Equation 15

Where f and h are nonlinear functions representing the state transition and measurement models, respectively, x_k is the state vector at time step k, u_k is the control input, w_k process noise. z_k is the measurement vector, v_k is measurement noise. The EKF operates in two main steps: prediction and update:

1. Prediction Step
2. The state and covariance matrix are propagated forward using the nonlinear system model.
3. Update Step
4. The measurement update uses the nonlinear measurement model to refine the state estimate.

By linearizing the nonlinear functions f and h around the current estimate, the EKF maintains a Gaussian approximation of the state distribution, allowing it to estimate the states of nonlinear systems effectively. However, the performance of EKF is highly sensitive to the accuracy of the linearization and initial estimates, as errors may propagate through the iterative process.

2.3 Loosely Coupled Integration Scheme

Loosely Coupled Integration uses the position and velocity data from GPS as the inputs to compensate for the errors identified in IMU [23]. The method usually uses a cascading scheme where GPS measurements including code, doppler, and phase are first processed to obtain the position, velocity, and orientation before being forwarded to the fusion algorithm. The three information are normally used to correct IMU errors while the covariance matrix from GPS data processing is also transferred to the fusion algorithm [24]. Moreover, Loosely Coupled is a type of range-domain integration that is relatively easy to implement based on different GPS/IMU sensor specifications. This has led to the wide application in the development of low-cost-based GPS/IMU integrations. GPS/IMU was chosen because it showed better results than GPS alone. This is because GPS measurements are easily disrupted by external influences such as multipath, while GPS-IMU remains continuous and robust. GPS and INS have complementary strengths and weaknesses, allowing them to work together to achieve accurate measurements [25].

IMU accelerometer and gyroscope generate specific forces and angular velocities. Furthermore, position, speed, and attitude tend to be obtained when applying the strap-down algorithm. In GPS module, observation procedures were conducted to detect the position and speed using SPP and DGPS methods. Moreover, DGPS method usually adopts GPS measurement and CORS SBY data as rover and base station, respectively. The difference in position and velocity between IMU and GPS was used as the input for Kalman Filter while other relevant information was stored during the filtering process. An integration algorithm was later used to determine the estimation of the error state associated with the inertial navigation system, and this was further applied to correct the initial IMU value. Furthermore, all the latest information was stored in the entire filtering process for smoothing. GPS/IMU integration system also implemented a closed-loop feedback correction to maintain error states and ensure optimism. The results of Loose Coupled integration concerning the position, speed, and attitude tended to be highly accurate and stable.

2.4 NearestSDP Function Principle

In UKF implementation, it is crucial to maintain the symmetry and positive semi-definiteness (SPD) of the covariance matrix throughout the filtering process. However, due to floating-point inaccuracies or computational errors, the matrix may lose its SPD property, which can lead to numerical instability, particularly during Cholesky decomposition. To address this, we utilized the nearestSPD function, which projects the computed covariance matrix to the nearest symmetric positive semi-definite matrix. This approach enhances the robustness of the UKF and ensures stable filtering performance. The nearestSPD method, originally developed [26], has been implemented in MATLAB [27] and is available in the MathWorks File Exchange. This function performs matrix symmetrization and adjusts eigenvalues to obtain the closest SPD matrix. The nearestSPD function operates by calculating the closest SPD matrix to the input covariance matrix, thereby preventing numerical errors that can arise from covariance matrix invalidity during the UKF update steps [26][27] and [28].

3. Methodology

This study was conducted in Institut Teknologi Sepuluh Nopember (ITS) area known as the Research Center Building, Surabaya City, presented in Figure 2, and data were collected using a Low-Cost Drone equipped with RPLiDAR.

Tarot 650 Iron Man drone was equipped with a payload system to carry a multi-sensor payload consisting of GPS, LiDAR, and IMU. The low-cost LiDAR drone was a quadcopter type which was considered more adaptive in maneuvering and equipped with a payload box consisting of a larger capacity compared to low-cost drones previously circulating on the market. The low-cost GNSS module used in this study follows a similar approach to the GNSS OEM boards evaluated by [29], who demonstrated that inexpensive GNSS sensors such as BX316 and K706 can produce stable and accurate positional data when compared to geodetic-grade receivers. The capacity allowed the drone to carry multiple sensors at once including GPS and LiDAR as well as IMU and gimbal added to support accurate positioning. Moreover, LiDAR data acquisition low-cost LiDAR (RPLiDAR A1M8-R6) type has an object scanning sensor using 2D laser light which can scan within a distance of 12 m at an angle range of 360 degrees. The 2D data obtained from the process can be used for mapping, localization, and environmental modeling. Furthermore, low-cost LiDAR (RPLiDAR A1) scanning frequency reaches 5.5 Hz which is adjustable up to a maximum of 10 Hz and capable of scanning up to 360 samples per rotation. Figure 3 shows the UAV equipped with several important components labelled with red arrows, including Low Cost GPS, which serves as the GPS module for UAV positioning; Propeller, which functions as the rotor blades to generate lift; Payload and IMU, which house the IMU sensor for measuring UAV motion and orientation; Low Cost LiDAR, which is used for collecting point cloud data, and Gimbal, which acts as a stabilizing mechanism to ensure accurate sensor measurements.

Figure 2: Institut Teknologi Sepuluh Nopember (ITS), Surabaya city

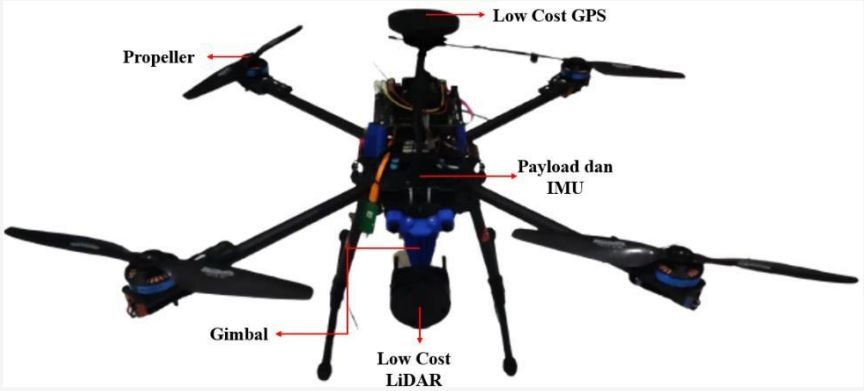

Figure 3: Tools setup for GPS/IMU/LiDAR data acquisition model

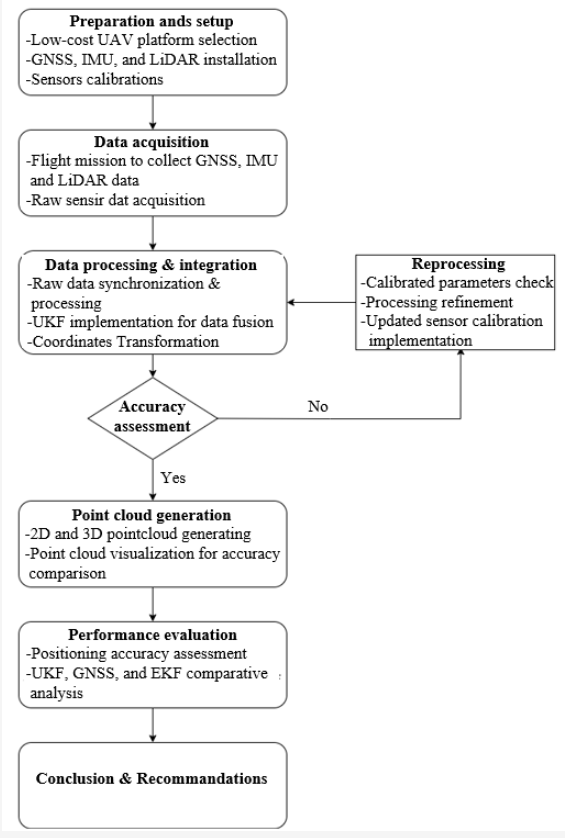

Figure 4: Workflow of Study

Data were acquired through a single flight mission, resulting in 27,112 epochs containing the following parameters: Date, Time, Roll angle (φ), Pitch angle (θ), Yaw angle (ψ), Altitude, Latitude, Longitude, and Compass heading. The orientation parameters Roll (φ), Pitch (θ), and Yaw (ψ) represent the rotational angles around the x-, y-, and z-axes, respectively, and are measured in radians. These orientation values were calibrated and subsequently visualized using a spatial data processing application.

The overall workflow of this study is summarized in Figure 4 and includes the following steps: (1) preparation and setup of the UAV platform, including the installation and calibration of GNSS, IMU, and LiDAR sensors; (2) data acquisition through flight missions to collect GNSS, IMU, and LiDAR data; (3) data processing and integration, which involves synchronization, preprocessing, and the implementation of the UKF for fusing GPS/IMU data, followed by coordinate transformation into the local LiDAR system; (4) an accuracy check to verify the positional accuracy of the fused data; (5) if necessary, reprocessing or recalibration of sensor data; (6) point cloud generation and visualization of 2D and 3D point clouds; (7) performance evaluation through statistical analysis and comparative assessment of UKF, GNSS, and EKF methods; and (8) concluding with recommendations for future improvements.

4. Results and Discussion

4.1 Performance of UKF and Comparation to EKF

UKF was stabilized using the 'nearestSPD' function to minimize instability in calculating the root of the P matrix via Cholesky decomposition, addressing issues when the P matrix became negative definite [21]. This approach ensured the matrix remained symmetric and positive definite, enhancing the stability of the UKF simulation. Additionally, GPS data were fused with IMU data to convert position information from the e-frame to the n-frame, aligning with the LiDAR's local coordinate system [22]. This transformation was crucial as the measurements tied to the GPS coordinate system needed to be compatible with the LiDAR system. These modifications made the UKF simulation more robust. The modeling of UAV motion and the compilation of UKF algorithm in MATLAB software were followed by simulations conducted to test the performance of the system and measurement model produced through the fusion of GPS and IMU

sensor data. The results obtained from UKF simulation trajectory are presented Figure 5.

Figure 5 illustrates the simulation results of the UAV quadrotor trajectory estimated using the UKF algorithm. Figure 5(a) presents the 2D trajectory in the horizontal plane (East-North), while Figure 5(b) shows the 3D trajectory in the East-North-Up coordinate system. The UKF estimation results are depicted using dashed lines, whereas the observation data are represented with solid lines. The cyan square and green star symbols indicate the UAV's starting and ending positions, respectively. Figure 5 demonstrates the consistency between the UKF estimation and the observation data in both 2D and 3D trajectories.

The visual representation of the results showed that the estimation using UKF simulation were close to the actual data. This provided qualitative evidence that estimation results of UKF were good and accurate. Meanwhile, the quantitative aspect was assessed through the calculation of Maximum Residual and RMSE. In Scenario I, the UKF utilized attitude data (orientation angles), resulting in more accurate 3D position estimates.

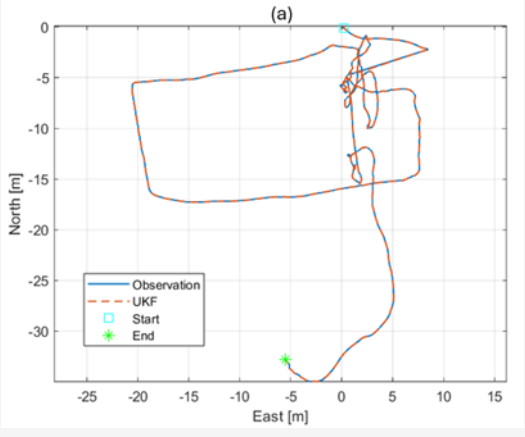

Figure 5: Trajectory of UKF simulation on a UAV (a) top view (b) 3D view

Although there was a relatively large maximum residual on the Y axis (20.421 m), the position RMSE values were relatively small, indicating that most estimates were close to the true position. The large maximum residual could be caused by temporary disturbances or sensor noise. In Scenario II (without attitude data), the 3D position errors were larger because the filter lacked orientation information to help improve position prediction. This highlights the importance of attitude data in enhancing the accuracy and stability of position estimation. These results align with previous research [13], which demonstrated that integrating attitude data into the UKF can achieve position accuracy within a few centimeters. Similarly, the research by [29] found that low-cost GNSS systems, when tested under RTK and PPP configurations, were capable of achieving centimeter-level accuracy compared to high-grade geodetic instruments, supporting the feasibility of cost-efficient sensor fusion in UAV mapping workflows.

Table 1: UKF simulation statistical values

Variable	RMSE (m)	Maximum residual
x	0.026	1.332 m
y	0.392	20.421 m
z	0.089	4.385 m
φ	2.804	36.026 rad
θ	0.249	2.513 rad
ψ	8.363	94.957 rad
P	0.212	9.128 rad/s
Q	0.164	4.353 rad/s
R	0.174	3.031 rad/s

The accuracy in Table 1 was calculated using the resultant squared RMSE of each variable. The samples with more than 100 data required reconstructing an error distribution close to the actual data with a standard deviation of 5% [30], thereby leading to more reliability. The results showed that UKF simulation achieved the 2D position accuracy of 0.403 m. This is supported by research results showing that the integration of GNSS and IMU using EKF produces higher RMSE values compared to other scenarios. The research results mention that UKF simulation produces better 2D accuracy compared to EKF estimation, which only achieves an accuracy value of 0.4132 m. Figure 6 is not much different from the results of the research conducted. Although the accuracy of EKF is lower than the accuracy value produced by UKF simulation, EKF shows a smoother trajectory visually than UKF. This is due to the elimination process in EKF [13].

Moreover, the performance was further tested by checking each measurement variable against time or epoch. The results obtained for the estimation of the position data (x, y, z) against time are presented in Figure 6.

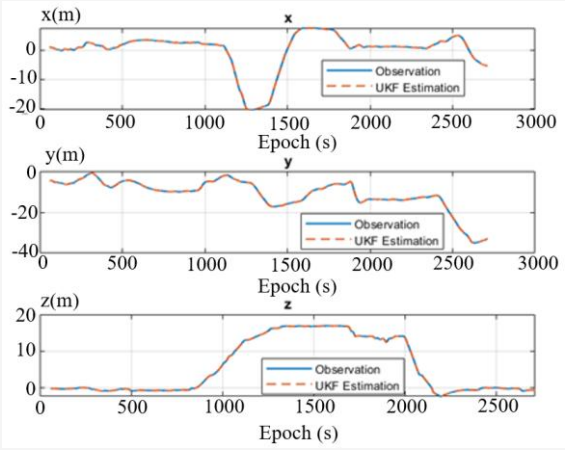

Figure 6: Comparison of UKF simulation results with position measurement data

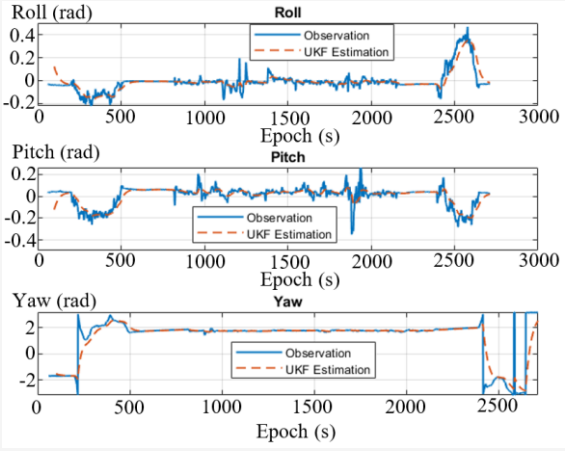

Figure 7: Comparison of UKF simulation results with attitude measurement data

The EKF estimation was applied to the fused GPS and IMU sensor data using Geopointer software, demonstrating that the processing did not necessitate UAV motion characterized by dynamic and kinematic models. The methodology emphasized the distribution of states as Gaussian random variables and their propagation through first-order linearization of the nonlinear system [31]. While the EKF has been successfully utilized in various applications, it is not without its limitations. These shortcomings prompted its inclusion in this study as a comparative framework for evaluating the performance of the UKF simulation, as depicted in Figure 7 and Figure 8. It is noteworthy that the EKF processing implemented via Geopointer software employed a distinct data structure compared to the UKF simulation conducted using the Matlab-based approach.

In addition to the comparison of UAV trajectories, it was also necessary to compare each variable from EKF estimation to the measurement data on X axis, Y axis, and Z axis with a focus on only the position as presented in Figure 9. This was because the variables were the same and could only be assessed based on the position data. The other data were not included due to the fact that the data were obtained from only the measurements or processes conducted. The comparison graph in Figure 9 shows that the estimated results of X axis (East) and Y axis (North) positions did not experience significant deviations, but Z axis in EKF Geopointer showed quite significant deviations. This was in line with a study that tested the performance of EKF fusion on position, speed, and attitude of the i-Boat navigation vehicle using Geopointer software [27]. It was discovered that EKF fusion was only able to achieve an accuracy of 0.413 m compared to UKF fusion with 0.040 m.

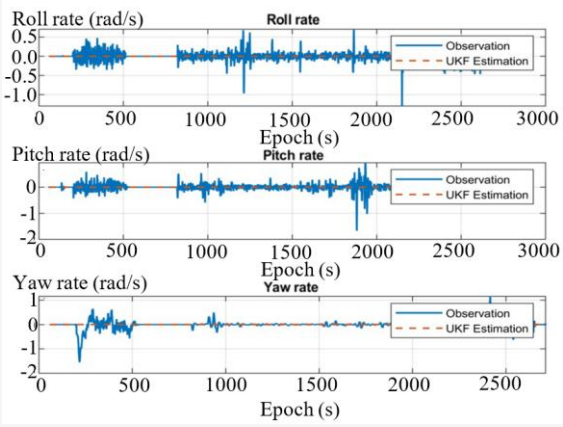

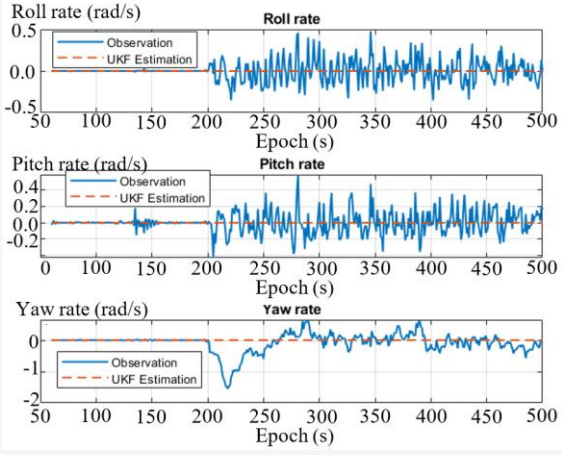

Figure 8: Comparison of UKF simulation results with angular velocity measurement data

The results in Table 2 indicate that the accuracy of position estimation using EKF varies across different axes, with the lateral axis showing better average accuracy compared to the longitudinal and vertical axes. However, despite the better average accuracy on the lateral axis, there is a notable potential for sudden large errors that can affect the overall stability of the estimation. In contrast, errors along the longitudinal axis tend to be more consistent and evenly distributed, although with relatively lower accuracy. This suggests that the estimation system should focus on mitigating temporary disturbances on the axis with the best average performance while also improving the consistently higher errors on the other axes to achieve optimal and stable position estimation results. Such an approach is crucial for enhancing the reliability of navigation or monitoring systems relying on EKF, especially in dynamic and noisy environments. To further illustrate the performance differences between the UKF and EKF methods, Figure 10 shows the overlay of their respective 2D trajectories. The overlay plot comparing the UKF and EKF trajectories reveals important insights into the performance differences between the two filtering methods.

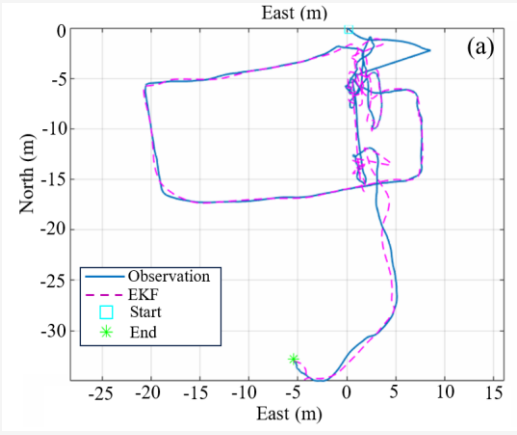

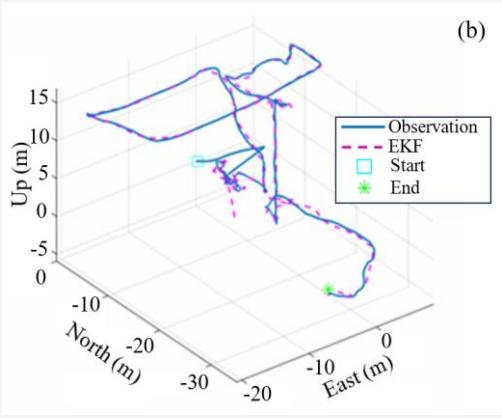

Figure 9: Trajectory of EKF simulation on a UAV quadrotor: (a) 2D trajectory and (b) 3D trajectory

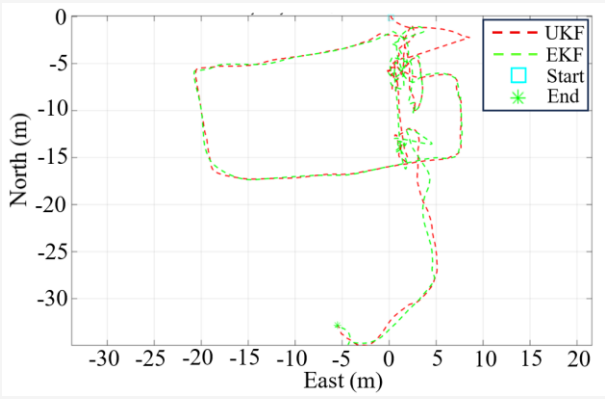

Figure 10: Comparison of 2D UAV trajectories derived from UKF and EKF estimations

Table 2: RMSE and maximum residual results for EKF simulation

Variable	RMSE (m)	Maximum residual (m)
X	1.859	26.767
Y	3.672	29.799
Z	3.635	18.879

Table 3: Differences in stand-alone GPS coordinates with UKF fusion results

No	Positioning difference between Stand alone and UKF fusion		
	X (m)	Y (m)	Z (m)
1	0.011	0.000	0.001
2	0.011	0.000	0.001
3	0.000	0.000	0.002
4	0.000	0.000	0.003
5	0.000	0.000	0.003
6	0.276	0.020	1.277
7	0.177	0.050	0.432
8	0.078	0.110	0.470
9	0.000	0.020	0.183
10	0.000	0.000	0.009

The UKF trajectory demonstrates smoother and more consistent estimation with less oscillation and noise compared to the EKF trajectory, particularly in the sections with sharp turns and abrupt motion changes. This indicates that the UKF is more robust in handling nonlinearities and dynamic maneuvers of the UAV. In contrast, the EKF trajectory shows more pronounced fluctuations and occasional deviations from the expected path, suggesting that it is more sensitive to measurement noise and less capable of handling abrupt changes in motion dynamics. Overall, this comparison highlights the advantages of using the UKF for accurate and stable UAV position estimation in challenging scenarios.

4.2 LiDAR Visualization

The coordinates produced from GPS/IMU sensor fusion and calculations with LiDAR data were used to determine the point cloud of the object. The point cloud obtained from GPS coordinate measurements (stand- alone), UKF and EKF fusion coordinates were visualized and compared. The RPLiDAR point cloud produced by Stand Alone GPS data before fusion and the UKF simulation was not significantly different as visually presented in Figure 10. Meanwhile, the coordinate positions of the fused model simulation were different from the Stand Alone GPS as presented in the following Table 3 using 10 sample data. The color ramp in Figure 10 represents the spatial variation of positional differences or accuracy values between sensor fusion results and reference data. Specifically, it visualizes the magnitude of coordinate deviations or residual errors in the fused GPS/IMU position data used for generating the 3D point cloud from LiDAR measurements. Colors at one end of the ramp indicate lower positional errors (higher accuracy), while colors at the opposite end indicate larger deviations (lower accuracy).

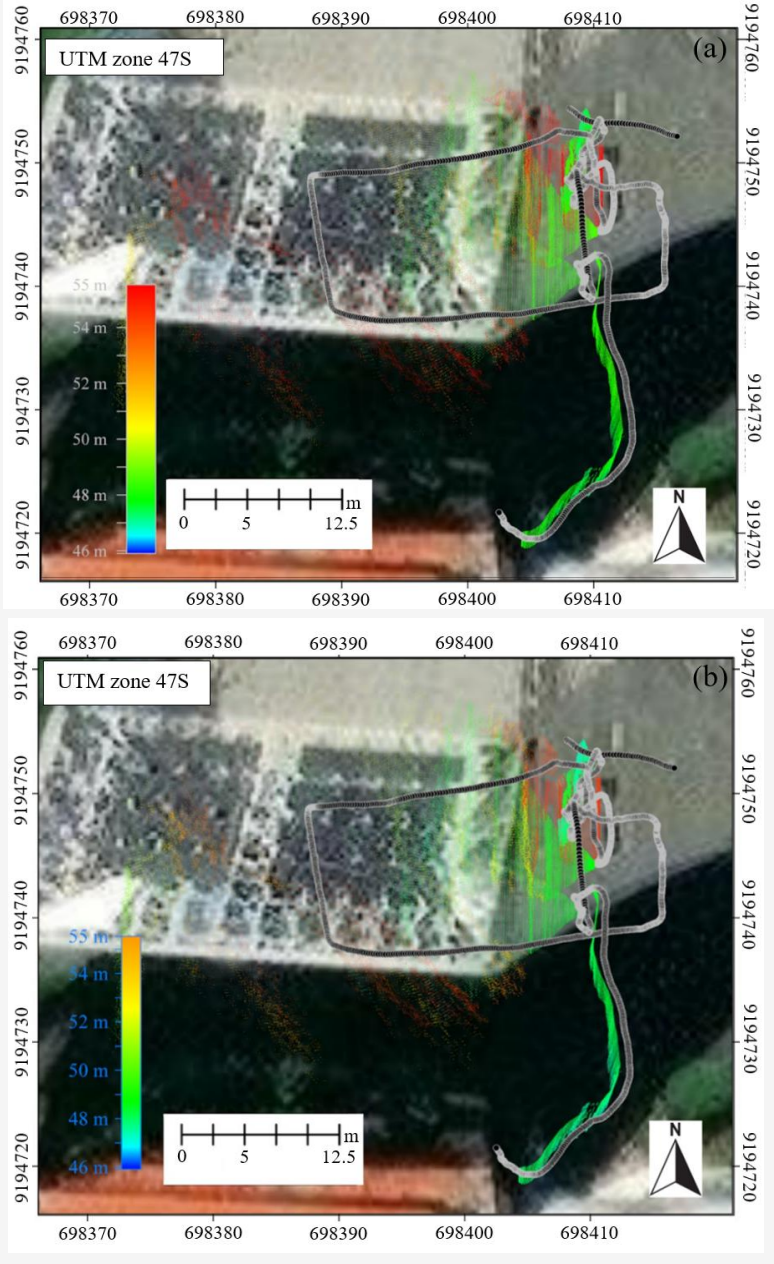

Figure 11: RPLiDAR point clouds derived from: (a) stand-alone GPS (b) UKF fusion

This color coding facilitates an intuitive visual understanding of the distribution of positional accuracy across the mapped area, supporting the quantitative analysis provided by the RMSE and maximum residual values detailed in the manuscript. The observed higher deviations in the X and Z coordinates at points 6 and 7, compared to other measurement points, are likely due to several factors. These points occurred during the UAV's ascent phase and were near tall buildings, which means point 6 and 7 were recorded when the drone was ascending and close to tall buildings this condition increased the likelihood of signal multipath and IMU drift.

Environmental conditions, such as wind and signal interference, as well as temporary fluctuations in sensor performance, may have contributed to these discrepancies. Additionally, although the integration of GPS and IMU sensors using the UKF generally improves accuracy, the IMU sensors, specifically the accelerometer and gyroscope, are susceptible to noise, particularly under certain flight conditions. This noise can lead to sensor drift, which was more noticeable along the X and Z axes at points 6 and 7. Furthermore, while the UKF algorithm efficiently filters sensor data, it remains sensitive to sudden changes in sensor readings, which may explain the higher residuals observed at these points [32]. A description of the specific location and flight phase (ascent and proximity to tall buildings) has also been included to provide clearer context to the observed deviations.

The point cloud coordinates showed minimal differences, reaching fractions of a millimeter, when UKF was fused with GPS. Along X axis, the majority of UKF fusion point cloud coordinates had closely similar values with GPS measurements but some deviations were recorded on Z axis due to the inherent instability of data, specifically in UAV used in acquiring data in the open air. This was in line with previous findings showing that the yaw attitude data on the Z axis were the most challenging to observe in vehicle movement [32]. The issue was discovered through the gyroscope measurement bias of Z axis which required a prolonged stabilization period. The RMSE values presented in Table 4 and the overall accuracy reported below were calculated during the UAV's ascent phase, when positioning accuracy is critical due to changing dynamics.

The UKF fusion coordinates achieved an overall 3D LiDAR point cloud accuracy of 0.034 m, with RMSE values of 0.007 m, 0.005 m, and 0.032 m recorded for the X, Y, and Z axes, respectively. This indicates that the Y axis exhibited the highest accuracy, while the Z axis showed the lowest. For comparison, the GPS stand-alone solution was used to evaluate method accuracy, with results showing that in some instances on the Y and Z axes, GPS stand-alone performed slightly better than UKF. Moreover, the UKF processing procedure is more complex and, in some cases, showed slightly less accuracy, particularly on the Y axis. An error reaching 0.036 m was detected in the UKF computation on the Z axis at epoch 3, likely related to specific conditions during data acquisition. The RMSE values for GPS, EKF, and UKF presented in Section 3 are now divided into two distinct phases, as shown in Tables 4 representing the UAV's pre-flight (ascent) and descent flight conditions, respectively. This division is essential because the UAV experiences different dynamic behaviors and environmental influences during ascent and descent, which significantly affect GNSS signal quality and positioning accuracy.

Table 4 (ascent phase) shows that the UKF fusion method produces smaller residuals across all axes compared to standalone GPS and EKF, with the X-axis residual reduced from 0.021 m (GPS) and 1.8590 m (EKF) to 0.3049 m (UKF). Similarly, the Y and Z axes also demonstrate lower residuals under UKF during ascent. Table 4 (descent phase) reveals a similar trend, where UKF maintains better accuracy and lower RMSE values compared to GPS and EKF, despite increased UAV dynamics during descent. Specifically, on the X-axis, UKF's residual is reduced from 0.021 m (GPS) and 4.2211 m (EKF) to 0.1055 m (UKF). On the Y-axis, UKF shows a residual of 0.1757 m, compared to 0.002 m (GPS) and 17.9598 m (EKF). For the Z-axis, UKF achieves a significant reduction, showing only 0.0246 m, while GPS and EKF show residuals of 0.006 m and 15.1340 m, respectively. This analysis confirms that UKF performs better in both ascent and descent phases, reducing positioning errors significantly compared to the other methods, especially in challenging dynamic conditions during descent.

The need for analyzing ascent and descent phases separately arises from significant differences in UAV movement patterns and external conditions affecting signal reception. Ascent generally involves steady altitude gain with relatively consistent acceleration, while descent includes more complex maneuvers and velocity changes, contributing to increased multipath effects and cycle slip occurrences. Cycle slips, which refer to the loss of phase continuity in GPS signals, tend to occur more frequently during rapid changes in the UAV's velocity, which can be particularly pronounced during ascent and descent phases. This is due to the increased dynamic movement during these phases, which amplifies the effects of cycle slips, ultimately degrading the accuracy of GPS signals. Furthermore,

the presence of buildings near the research location exacerbates these effects, as they introduce additional multipath interference. The illustrative trajectories in Figure 11 support this observation by highlighting distinct variations in signal behavior between these flight phases, confirming that UAVs undergo more frequent cycle slip events during ascent and descent compared to horizontal flight. These findings align with the research [33], which discuss the impact of dynamic environments on cycle slip detection in GNSS/INS systems, and [34], which highlight the challenges of cycle slip occurrence in low-elevation data, particularly in environments with multipath interference, such as those near buildings.

Table 4: Comparison of Position RMSE Values (in meters) for Each Coordinate Axis (X, Y, Z) Using Stand-alone GPS, Extended Kalman Filter (EKF), and Unscented Kalman Filter (UKF) Processing Methods under Pre-flight UAV Conditions and under UAV Descent Conditions

Axis	RMSE (m)		
	Stand alone	EKF	UKF
Ascent phase			
X	0.021	1.859	0.305
Y	0.002	3.672	0.127
Z	0.006	3.635	0.068
Descent phase			
X	0.021	4.221	0.106
Y	0.002	17.960	0.176
X	0.006	15.134	0.025

Furthermore, the volume increment of 28.92% indicates the improvement in 3D volumetric reconstruction accuracy achieved by using UKF-based GPS/IMU fusion compared to EKF. In this study, volume refers to the three-dimensional (3D) space enclosed by the reconstructed point cloud model of the observed object. This volume was calculated from the fused point cloud data, providing a quantitative assessment of the spatial representation accuracy. The 28.92% increase indicates that the UKF fusion produced a more complete and accurate 3D point cloud, resulting in a larger and more precise estimated object volume than the EKF. This result confirms the advantage of the UKF method in 3D mapping applications, especially when high-fidelity spatial measurements are required.

These findings emphasize UKF's advantage for sensor fusion in dynamic UAV operations. As demonstrated in both ascent and descent phases, UKF achieves the lowest RMSE across all coordinate axes, confirming its suitability for enhancing 3D positioning accuracy in LiDAR point cloud applications, particularly along the X-axis. Therefore, the UKF method stands out as the preferred choice for reliable and precise UAV navigation and mapping. Additionally, the LiDAR sensor showed reliable performance in measuring distances and maintained low speed estimation errors, indicating its suitability for accurate positioning within safe operating distances [35]. Room mapping through RPLiDAR using a mobile robot had a scanning accuracy above 90% and between 5 to 11 m [36]. The outdoor mapping conducted in this study through the application of the 2D RPLiDAR had a position accuracy of 7-32 cm which was in line with the results reported by [36].

The accuracy of standalone GPS positioning is contingent upon the quality of satellite signals and the surrounding environment. In open and unobstructed outdoor areas, standalone GPS receivers are capable of directly calculating three-dimensional positions by utilising signals from multiple satellites. In such ideal conditions, these devices frequently attain excellent accuracy due to minimal disturbance to the signals [37]. Indeed, standalone GPS frequently yields superior results when signal conditions are optimal, such as in open outdoor areas without obstructions, because it can calculate position directly from four or more satellites, allowing precise 3D positioning. In such circumstances, standalone GPS has been shown to outperform sensor fusion methods by avoiding errors that may arise from sensor noise or the complexities involved in data fusion. Conversely, the UKF fusion method integrates GPS data with inertial measurements from IMUs to enhance positioning reliability, particularly in environments where GPS signals are degraded by obstructions or multipath effects, such as urban canyons or dense forests [38].

The IMU provides high-frequency updates on velocity and orientation, enabling continuous navigation even in the event of temporary unavailable GPS signals. However, the performance of UKF fusion is contingent on the quality of the IMU sensors. In the field of precision engineering, IMUs are susceptible to drift, a phenomenon attributed to sensor biases and the accumulation of noise. This drift can lead to the growth of errors over time if external correction from GPS is inadequate [35]. Despite the fact that IMUs provide valuable velocity and orientation data for position determination, their drift causes an increase in positional deviations during extended GPS outages.

5. Conclusion

This study demonstrated that the fusion of GPS and IMU sensors on a Low-Cost Quadrotor UAV using the UKF method achieved an overall measurement accuracy of 0.403 m. The UKF method consistently outperformed the Extended Kalman Filter (EKF) and standalone GPS, delivering significantly lower RMSE values across all coordinate axes during both UAV ascent and descent phases. The results indicate that the EKF method experiences a notable increase in RMSE values during the UAV landing phase, with errors growing by a factor of 2 to nearly 5 compared to the UAV hover phase, especially along the Y and Z axes. In contrast, the UKF method maintains relatively stable RMSE values, even showing slight decreases on the X and Z axes under landing conditions, demonstrating better robustness and accuracy in dynamic flight scenarios. The standalone GPS, while consistent across both flight phases, lacks the adaptability of sensor fusion methods to effectively cope with challenging and changing environments.

The UKF method is essential for integrating 3D LiDAR data with UAV navigation, as it ensures consistent accuracy in point cloud mapping, not only for UAV positioning but also for the overall mapping process. The combination of 3D LiDAR and UKF improves measurement reliability and ensures that spatial data is accurately referenced to the UAV's position. This is particularly beneficial for low-cost drone mapping, where sensor fusion can compensate for occasional GPS signal loss and improve mapping results. A key finding of this research is the UKF's ability to maintain stable and reliable positioning in challenging environments, particularly in areas prone to frequent cycle slips and signal degradations. By effectively fusing IMU data with GPS, UKF produces a denser and more reliable 3D LiDAR point cloud, which directly translates to an improved volume estimation accuracy. Specifically, the volume calculations based on UKF fusion increased by 28.92% compared to those based on EKF, highlighting UKF's significant advantage in generating high-fidelity volumetric spatial data.

These improvements are critical for applications requiring precise 3D mapping, such as environmental monitoring, resource management, and precision agriculture, where accurate volumetric measurements are essential. Despite these promising results, further studies are necessary to optimize sensor calibration procedures under varying environmental conditions and to evaluate sensor performance more comprehensively in real operational scenarios. Additionally, expanding the use of 3D LiDAR mapping in outdoor environments will further benefit from UKF's robustness, enabling the generation of even denser and more accurate point clouds.

In summary, the UKF-based sensor fusion approach presents a scalable and effective solution for enhancing UAV navigation and mapping performance, especially on low-cost platforms. Its capacity to handle nonlinearities, sensor noise, and signal interruptions makes it highly suitable for real-world applications demanding reliable and precise spatial data acquisition.

Acknowledgments

The authors gratefully acknowledge financial support from the Institut Teknologi Sepuluh Nopember for this work, under project scheme of the Publication Writing and IPR Incentive Program (PPHKI) 2025.

References

[1] Khan, S.I., Ahmed, A. and Li, Y., (2021). UAVs Path Planning Architecture for Effective Medical Emergency Response in Future Networks. *Physical Communication*, Vol. 47. https://doi.org/10.1016/j.phycom.2021.101337

[2] Rieke, M., Dittmann, A. and Bielecki, C., (2012). High-Precision Positioning and Real-Time Data Processing of UAV-Systems. *The International Archives of the Photogrammetry, Remote Sensing and Spatial Information Sciences*, Vol. 38, 119–124.

[3] Khamseh, H. B., Ghorbani, S. and Janabi-Sharifi, F., (2019). Unscented Kalman Filter State Estimation for Manipulating Unmanned Aerial Vehicles. *Aerospace Science and Technology*, Vol. 92; 446–463. https://doi.org/10.1016/j.ast.2019.06.003.

[4] Cahyadi, M. N. and Rwabudandi, I., (2019). Integration of GPS-IMU for Increasing the Observation Accuracy in Condensed Areas (Infrastructure and Forest Canopies). *E3S Web of Conferences*, Vol. 94. https://doi.org/10.1051/e3sconf/20199403015.

[5] Ollander, S., Bode, F. W. and Baum, M., (2018). Multi-Frequency GPS Signal Fusion for Minimization of Multipath and Non-Line-of-Sight Errors: A Survey. 2018 15th Workshop on Positioning, Navigation and Communications (WPNC). *IEEE*. https://doi.org/10.1109/WPNC.2018.8555856.

[6] Cahyadi., M. N., Bawasir, A., Arief, S., Widodo, A., Rusli, M., Kusumawardani, D., Rahmawati, Y., Martina, A., Maulida, P. and Lestiana, H., (2024). Analysis of the Effect of the 2021 Semeru Eruption on Water Vapor Content and Atmospheric Particles Using GNSS and Remote Sensing. *Geodesy and*

Geodynamics, Vol. 15, 33-41. https://doi.org/10.1016/j.geog.2023.04.005.

[7] Chu, H. J., Tsai, M. J., Chang, T. Y. and Chen, K. S., (2013). GPS/MEMS INS Data Fusion and Map Matching in Urban Areas. *Sensors*, Vol. 13(9); 11280–11288. https://doi.org/10.3390/s130911280.

[8] Meng, X., Wang, H. and Liu, B., (2017). A Robust Vehicle Localization Approach Based on GPS/IMU/DMI/LiDAR Sensor Fusion for Autonomous Vehicles. *Sensors*, Vol. 17(9). https://doi.org/10.3390/s17092140.

[9] Stetzel, K. D., Klein, R. and Park, S., (2015). Electrochemical State and Internal Variables Estimation Using a Reduced-Order Physics-Based Model of a Lithium-Ion Cell and an Extended Kalman Filter. *Journal of Power Sources*, Vol. 278; 490–505.

[10] Pérez, G., Garmendia, M., Reynaud, J. F., Crego, J. and Viscarret, U., (2015). Enhanced Closed Loop State of Charge Estimator for Lithium-Ion Batteries Based on Extended Kalman Filter. *Applied Energy*, Vol. 155; 834–845.

[11] Li, Q., Wang, H. and Liu, J., (2015). Kalman Filter and Its Application. *2015 8th International Conference on Intelligent Networks and Intelligent Systems (ICINIS).* IEEE.

[12] Nemra, A. and Aouf, N., (2010). Robust INS/GPS Sensor Fusion for UAV Localization Using SDRE Nonlinear Filtering. *IEEE Sensors Journal*, Vol. 10(4), 789–798.

[13] Cahyadi, M. N., Asfihani, T., Mardiyanto, R. and Erfianti, R., (2022). Loosely Coupled GNSS and IMU Integration for Accurate i-Boat Horizontal Navigation. *International Journal of Geoinformatics*, Vol. 18(3); 111-122. https://doi.org/10.52939/ijg.v18i3.2233.

[14] Elamin, A., Abdelaziz, N. and El-Rabbany, A., (2022). A GPS/INS/LiDAR Integration Scheme for UAV-Based Navigation in GPS-Challenging Environments. *Sensors*, Vol. 22(24). https://doi.org/10.3390/s22249908.

[15] Uaratanawong, V., Tangvijitjankarn , K., and Satirapod, C. (2024). Performance of a Low-Cost GNSS Receiver Using MADOCA Corrections with Precise Point Positioning (PPP) Mode in Thailand. *International Journal of Geoinformatics*, Vol. 20(5), 69–78. https://doi.org/10.52939/ijg.v20i5.3233.

[16] Najm, A. A. and Ibraheem, I. K., (2019). Nonlinear PID Controller Design for a 6-DOF UAV Quadrotor System. *Engineering Science and Technology, an International Journal*, Vol. 22(4); 1087–1097.

[17] Giernacki, W., Bode, F. W. and Baum, M., (2021). Mathematical Modeling of the Coaxial Quadrotor Dynamics for Its Attitude and Altitude Control. *Energies*, Vol. 14(5). https://doi.org/10.3390/en14051232.

[18] Madathiparambil Jose, J., (2009). Performance Comparison of Extended and Unscented Kalman Filter Implementation in INS-GPS Integration. Master Thesis, Engineering Environment Science, Lulca University of Technology.

[19] Ryu, J., Moon, Y., Choi, J. and Kim, H. C., (2018). A Kalman-Filter-Based Common Algorithm Approach for Object Detection in Surgery Scene to Assist Surgeon's Situation Awareness in Robot-Assisted Laparoscopic Surgery. *Journal of Healthcare Engineering*, Vol. 2018. https://doi.org/10.1155/2018/5174853.

[20] Deng, Y., Chen, X. and Huang, Z., (2024). A Highly Powerful Calibration Method for Robotic Smoothing System Calibration via Using Adaptive Residual Extended Kalman Filter. *Robotics and Computer-Integrated Manufacturing*, Vol. 86. https://doi.org/10.1016/j.rcim.2023.102660.

[21] Ryu, K. and Back, J., (2019). *Distributed Kalman-Filtering: Distributed Optimization Viewpoint.* 2019 IEEE 58th Conference on Decision and Control (CDC). *IEEE.*

[22] Haykin, S., (2004). *Kalman Filtering and Neural Networks.* New York: John Wiley & Sons. Inc. https://doi.org/10.1002/0471221546

[23] Almagbile, A., Al-Rawabdeh, A., and Hazaymeh, K. (2023). Analysis of Single and Double Faults Direction and Magnitude in Measurement and State Models of Tight GPS/INS System. *International Journal of Geoinformatic*s, Vol. 19(7), 47–62. https://doi.org/10.52939/ijg.v19i7.2745.

[24] Petovello, M. G., Cannon, M. E. and Lachapelle, G., (2003). *Kalman Filter Reliability Analysis Using Different Update Strategies*. Proceedings of the CASI Annual General Meeting.

[25] Cahyadi, M. N. and Rwabudandi, I., (2019). Integration of GNSS-IMU for Increasing the Observation Accuracy in Condensed Areas (Infrastructure and Forest Canopy). *E3S Web of Conferences ISGNSS*. https://doi.org/10.1051/e3sconf/20199403015.

[26] Higham, N. J., (1988). Computing a Nearest Symmetric Positive Semidefinite Matrix. *Linear Algebra and its Applications*, Vol. 103; 103–118. https://doi.org/10.1016/0024-3795(88)90223-6.

[27] D'Errico, J., *NearestSPD: Nearest (Symmetric) Positive Definite Matrix.* MATLAB Central File Exchange. [Online]. Available: https://www.mathworks.com/matlabcentral/fileexchange/42885-nearestspd. [Accessed: Nov. 1, 2025].

[28] Salem, H., Ahmed, M., AlSharif, M., Muqaibel, A. and Al-Naffouri, T., (2025). *Indoor Position and Attitude Tracking with SO(3) Manifold.* arXiv preprint, arXiv:2501.01555. https://doi.org/10.48550/ar Xiv.2501.01555.

[29] Cahyadi, M. N., Handoko, E. Y., Anjasmara, I. M., Khomsin., Maulida, P., Ubaidillah, M. R. and Putra, M. E., (2020). *Comparative Analysis of Low-Cost GNSS OEM Board K706 and BX316 (Case Study: Bulusidokare Village Sidoarjo Regency). IOP Conference Series: Earth and Environmental Science*, 731(1). https://doi.org/10.1088/1755-1315/731/1/012024.

[30] Chai, J., Wu, C., Zhao, C., Chi, H. L., Wang, X., Ling, B. W. K. and Teo, K. L., (2017). Reference Tag Supported RFID Tracking Using Robust Support Vector Regression and Kalman Filter. *Advanced Engineering Informatics*, Vol. 32, 1–10. https://doi.org/10.1016/j.aei.2017.01.003.

[31] VanDyke, M. C., Schwartz, J. L. and Hall, C. D., (2004). Unscented Kalman Filtering for Spacecraft Attitude State and Parameter Estimation. *Advances in the Astronautical Sciences*, Vol. 118(1), 217–228.

[32] Xia, S., Wang, W., Li, S. and Wang, Z., (2016). *Application of Kalman Filter in Microseismic Data Denoising Based on Identified Signal Model.* 2016 Chinese Control and Decision Conference (CCDC). *IEEE.*

[33] Chai, D., Sang, W., Chen, G., Ning, Y., Xing, J., Yu, M. and Wang, S., (2022). A Novel Method of Ambiguity Resolution and Cycle Slip Processing for Single-Frequency GNSS/INS Tightly Coupled Integration System. *Advances in Space Research*, Vol. 69; 359–375. https://doi.org/10.1016/j.asr.2021.10.007.

[34] Liu, N., Zhang, Q., Zhang, S. and Wu, X., (2021). Algorithm for Real-Time Cycle Slip Detection and Repair for Low Elevation GPS Undifferenced Data in Different Environments. *Remote Sensing*, Vol. 13(11). https://doi.org/10.3390/rs13112078.

[35] Greco, C. and Vasile, M., (2021). *Fundamentals of Filtering.* Optimization Under Uncertainty with Applications to Aerospace Engineering. Cham, Switzerland: Springer.

[36] Markom, M. A., Adom, A. H., Tan, E. S. M. M., Shukor, S. A. A., Rahim, N. A. and Shakaff, A. Y. M., (2015). A Mapping Mobile Robot Using RP Lidar Scanner. 2015 IEEE International Symposium on Robotics and Intelligent Sensors (IRIS). *IEEE*.

[37] Cahyadi, M. N., Asfihani, T., Mardiyanto, R. and Erfianti, R., (2023). Performance of GPS and IMU Sensor Fusion Using Unscented Kalman Filter for Precise i-Boat Navigation in Infinite Wide Waters. *Geodesy and Geodynamics*, Vol. 14(3); 265–274. https://doi.org/10.1016/j.geog.2023.02.004.

[38] Deng, Y., Chen, X. and Huang, Z., (2024). A Highly Powerful Calibration Method for Robotic Smoothing System Calibration via Using Adaptive Residual Extended Kalman Filter. *Robotics and Computer-Integrated Manufacturing*, Vol. 86. https://doi.org/10.1016/j.rcim.2023.102660.